nature electronics

Article

https://doi.org/10.1038/s41928-024-01236-7

A fingertip-wearable microgrid system for autonomous energy management and metabolic monitoring

Received: 8 January 2024

Accepted: 31 July 2024

Published online: 3 September 2024

Check for updates

Shichao Ding[1,5], Tamoghna Saha[1,5], Lu Yin[1,5], Ruixiao Liu[1], Muhammad Inam Khan[1], An-Yi Chang[1], Hyungjin Lee[1], Han Zhao[2], Yuanzhe Liu[3], Ariane Sina Nazemi[2], Jiachi Zhou[1], Chuanrui Chen[1], Zhengxing Li[1], Chenyang Zhang[1], Sara Earney[1], Selene Tang[1], Omeed Djassemi[1], Xiangjun Chen[1], Muyang Lin[1], Samar S. Sandhu[1], Jong-Min Moon[1], Chochanon Moonla[1], Ponnusamy Nandhakumar[1], Youngmin Park[4], Kuldeep Mahato[1], Sheng Xu[1] & Joseph Wang[1]

Wearable health monitoring platforms require advanced sensing modalities with integrated electronics. However, current systems suffer from limitations related to energy supply, sensing capabilities, circuitry regulations and large form factors. Here, we report an autonomous and continuous sweat sensing system that operates on a fingertip. The system uses a self-voltage-regulated wearable microgrid based on enzymatic biofuel cells and AgCl-Zn batteries to harvest and store bioenergy from sweat, respectively. It relies on osmosis to continuously supply sweat to the sensor array for on-demand multi-metabolite sensing and is combined with low-power electronics for signal acquisition and wireless data transmission. The wearable system is powered solely by fingertip perspiration and can detect glucose, vitamin C, lactate and levodopa over extended periods of time.

Skin-interfacing wearable electronics are of potential use in a range of applications from health monitoring to human–machine interactions[1–4]. Wearable sensors can be used to measure different biological signals in real-time[5]. However, the widespread deployment of wearable electronics is restricted by a number of practical limitations including safety and biocompatibility, large device footprint, unreliable operation and inconvenient usage. Trade-offs are thus often made to satisfy some of the needs. For example, to reduce the need for batteries, wired or short-range wireless power supplies are used that restrict user mobility[6–9]. The use of rigid batteries in turn increases the device footprint, requires frequent battery charging or replacement, and creates a potential safety hazard[10–12]. Alternatively, wearable energy harvesters can be integrated, but with the system reliant on energy input from a specific external environment (such as light and temperature) or user activity (such as movement and exercise). This can increase complexity, requiring the addition of conversion and regulation circuits, which cause energy loss[13–26]. Furthermore, continuous sweat biomarker monitoring relies on either physical activity or electrical stimulation for sweat extraction[27–29], amplifying the energy investment and restricting the practicality and user-friendliness of such systems.

Recent work has illustrated the feasibility of creating a wearable microgrid system with compatible form factors, commensurate power rating and complementary characteristics between the sensing and energy modalities[18,30]. Such a system relies on integrating energy

[1]Aiiso Yufeng Li Family Department of Chemical and Nano Engineering, University of California San Diego, La Jolla, CA, USA. [2]Department of Electrical and Computer Engineering, University of California San Diego, La Jolla, CA, USA. [3]Department of Computer Science and Engineering, University of California San Diego, La Jolla, CA, USA. [4]Samsung Electronics, Suwon-si, Gyeonggi-do, Republic of Korea. [5]These authors contributed equally: Shichao Ding, Tamoghna Saha, Lu Yin. e-mail: josephwang@ucsd.edu

harvesting with energy storage capabilities with matching electrical characteristics to minimize energy loss during conversion, improve energy reliability and extend operation[22,31]. These energy systems should then be combined with electronics and sensing components with similar form factors and optimized for specific usage scenarios, thereby reducing the device footprint and improving practicality. The further development of wearable microgrids requires, in particular, addressing challenges related to sustainable autonomous power supply, miniaturization, self-regulation, on-demand multisensory biomarker detection, safety and comfortable wearability.

In this Article, we report an integrated fingertip-wearable microgrid system (Fig. 1). The system offers energy harvesting and storage abilities, as well as a multiplexed sensing system and electronic controller. Integration is achieved by addressing challenges related to placing the complete sensor arrays, energy modules and microcontroller unit (MCU) system onto a single finger and operating it efficiently without any physical movement (Fig. 1a). The system can capture energy from passively harvested sweat through self-regulated lactate-based biofuel cells (BFCs) without physical activity. By pairing these BFCs with stretchable silver chloride-zinc (AgCl-Zn) batteries, the fingertip microgrid can regulate and store the harvested bioenergy to power the MCU and the wearable multiplexed sensing system.

Fingertips have a high density of sweat glands (~400 glands per cm^{-2}) and rapid sweat secretion rates (50–500 nl min^{-1} cm^{-2})[32,33]. The composition of eccrine sweat includes around 99% water with electrolytes and key metabolites[34], which is dynamically dependent on the physiological state of the individual. These chemicals (biofuels and biomarkers) act as the source for biochemical energy[20] and can be monitored non-invasively for tracking varying metabolic conditions[27,32,35,36]. The fingertip sweat plays two roles in the wearable microgrid (Fig. 1b): first, to provide sustainable biofuel to the BFCs for harvesting biochemical energy at rest, and eventually supporting energy storage in the integrated stretchable AgCl-Zn battery module. Second, the osmotically extracted sweat supports non-invasive and dynamic self-powered sensing.

The rechargeable batteries extend the energy storage by harnessing the BFC-based harvested bioenergy and enable continuous multiplexed sensing of key metabolic biomarkers (glucose (Glu), vitamin C and lactate) and disease-related drugs (levodopa (L-dopa)). A low-power MCU controls the fingertip-mounted sensors, with the generated signal being sampled via an analogue-to-digital converter (ADC). This conversion process transforms the analytical data into digital outputs, and the resulting personalized diagnostics information is wirelessly transmitted to a user interface through Bluetooth low energy (BLE). The output information can be displayed on a smartphone or laptop, leading to a real-time personalized health status evaluation.

Design of the fingertip-wearable microgrid

The fingertip-wearable microgrid system consists of four BFCs, two AgCl-Zn batteries, a flexible printed circuit board (fPCB), four potentiometric electrochemical sensors and a hydrogel-based osmotic sweat pumping system with a laser-engraved paper microfluidic channel (Fig. 1a). The circuits, stretchable battery and sensors are printed layer-by-layer on a poly(styrene-b-(ethylene-co-butylene)-b-styrene) (SEBS) thermoplastic elastomer substrate (Fig. 1c and Supplementary Figs. 1 and 2). Porous carbon foams and hydrogels are used as the electrode and sweat collectors for the BFCs, respectively. The carbon foam is anchored to the current collector (made using stretchable silver inks (sAg)) using carbon glue. The high elastic nature of SEBS and sAg inks enables high mechanical resiliency of the microgrid system against undesirable physical deformations (Supplementary Fig. 3), allowing the entire system to be placed conformally around the fingertip (Fig. 1c). Scanning electron microscopy (SEM) images of sAg also indicate the absence of breakage under 20% stretching (Supplementary Fig. 4). Chloride and lactate acid treatment further enhances the stability of the sAg circuit (Supplementary Fig. 5)[37]. The fPCB is bonded on the printed circuits without compromising the elasticity via a rapid room-temperature solvent-welding method, without using any bonding layer or conductive pastes (Supplementary Fig. 6). The BFCs connected in series show an open-circuit potential (OCP) of 1.4 V and achieve their maximum power output at 1 V. This regulated voltage ensures that the BFCs consistently operate at their maximum power to enable successful charging of the AgCl-Zn battery (with a redox potential of approximately 1 V). Connecting two AgCl-Zn batteries in series generates a combined potential of around 2 V, which is sufficient to continuously power the MCU. The schematic illustration of the self-regulated power system and the circuit design is shown in Supplementary Fig. 7. Electrochemical sensors have been developed and assembled for the continuous potentiometric detection of Glu, vitamin C, lactate and L-dopa. A laser-engraved microfluidic paper channel supports osmotic pumping, which allows the fingertip sweat to be extracted efficiently during daily activities and guided towards the sensors[38]. The MCU collects the signals from the electrochemical sensors, transforms them to readable data via an ADC and transmits them through BLE for further analysis.

Characterization of BFC and battery

The fingertip energy management module is designed to incorporate the combined chemical properties of BFCs and AgCl-Zn batteries. The BFC chemistry and the battery have been carefully characterized to ensure matching operating potentials and complementary characteristics for commensurate performance. Here, the harvester modules were designed with a pair BFCs (each with a full cell OCP of 0.7 V) connected in series to provide commensurate voltage (~1.4 V) to charge a single AgCl-Zn battery. Soft, durable, conductive and porous carbon foams were designed and optimized for fabricating the BFC (Supplementary Figs. 8 and 9). The porous nature of carbon foam allows sufficient loading of the enzymes and corresponding chemicals (conducting materials, mediators, enzyme coupling regents) for boosting the energy density. The lactate oxidase (LOx)-based anode facilitates the oxidation of lactate into pyruvate, while the bilirubin oxidase (BOD)-based cathode carries out an oxygen reduction reaction (Fig. 2a and Supplementary Fig. 10a)[20,39]. The electrocatalytic activity and stability of the anode and cathode are attributed to the synergistic interaction of the mediators (1,4-naphthoquinone (NQ) or 2,2′-azino-bis(3-th ylbenzothiazoline-6-sulfonic acid (ABTS)), enzyme coupling regent (hemin)[40], carbon foam design and electrode capping layers for minimizing the leaching of components (Supplementary Figs. 10b,c and 11). The BFC module endures common mechanical deformations, such as bending, wrapping and stretching (Fig. 2b), by withstanding a typical 20% strain[41]. The performance of a single BFC was tested using linear scan voltammetry (LSV) at different lactate concentrations (from 5 to 35 mM), which are the typical physiological levels found in sweat[19,42–44]. The generated power increased proportionally with the lactate concentration (Fig. 2c). An in vitro experiment using 20 mM lactate solution was conducted to assess the performance of BFCs with various configurations. The single BFC demonstrated a maximum power output of approximately 250 μW at 0.5 V. However, when two BFCs were connected in series, the power output was enhanced to approximately 600 μW (Fig. 2d). Consequently, the entire four-BFC energy harvester module provided a peak power of ~1,200 μW at 1 V. A 10-min chronoamperometry measurement was further conducted to evaluate the BFC power during extended operations[18]. As shown in Fig. 2e,f, the current density (j) of a single BFC increases with rising lactate concertation at 0.5 V, reaching up to ~120 μA cm^{-2}. A 25 mM lactate concertation was used to investigate the BFC's ability to generate stable power, which corresponds to ~634 mJ energy after 10 h of extended operation (Fig. 2g). Also, BFCs connected in series ensures an OCP higher than 1.05 V for 12 days, which can further benefit long-time battery charging in the microgrid (Supplementary Fig. 10d).

https://doi.org/10.1038/s41928-024-01236-7

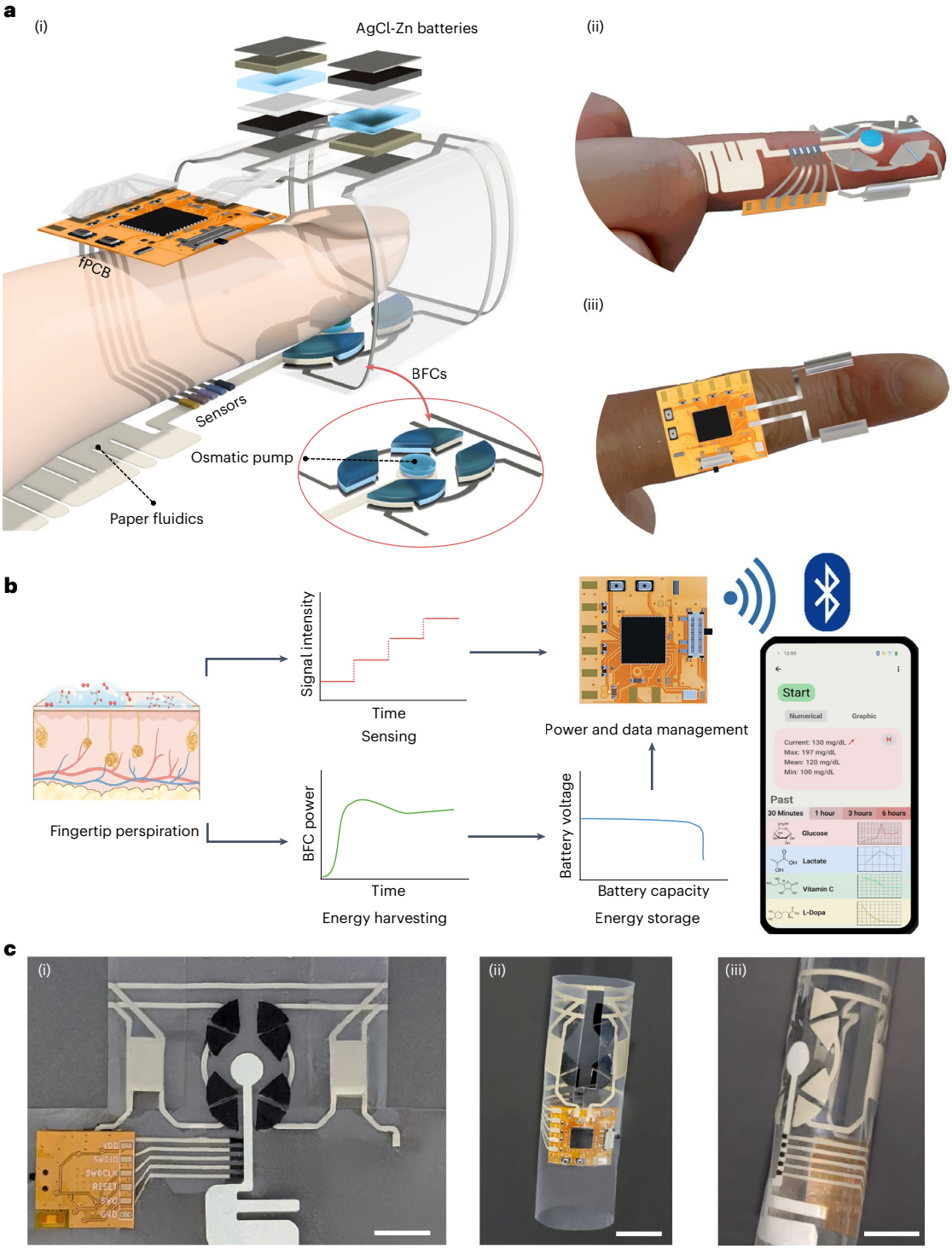

Fig. 1 | Principle and design of integrated fingertip-wearable microgrid. **a**, Schematic of the fingertip-wearable microgrid system, which includes BFCs, AgCl-Zn batteries, fPCB and wearable sensors with an osmotic sweat extraction assisted paper fluidic system. The combination of BFCs and AgCl-Zn batteries is constructed as an energy module, which comprises a serial connection of two AgCl-Zn batteries and each being charged by two serial-connected BFCs. The inset (in the red circle) is zoomed in on the components interfaced with the fingertip, which includes four BFCs and a centre osmotic pumping system for sweat extraction: (i) main schematic, (ii) ventral side and (iii) dorsal side. **b**, Schematic of the fingertip-mounted energy microgrid working principle for energy harvesting, energy storage and electrochemical sensing with wireless data transition and smartphone display. Fingertip perspiration provides biofuel and biomarkers for passive energy harvesting and continuous sensing, respectively. The powered MCU supports four sensors for metabolic monitoring, dietary supplements and drugs monitoring, which are associated with various physiological and metabolic conditions. **c**, Optical images of the fingertip-wearable microgrid. Outlooks of the expanded structure (i) before folding, (ii) after folding and connecting the BFC-battery to the fPCB, (iii) and after inclusion of a paper fluidic channel and sensors. Scale bars, 1 cm.

https://doi.org/10.1038/s41928-024-01236-7

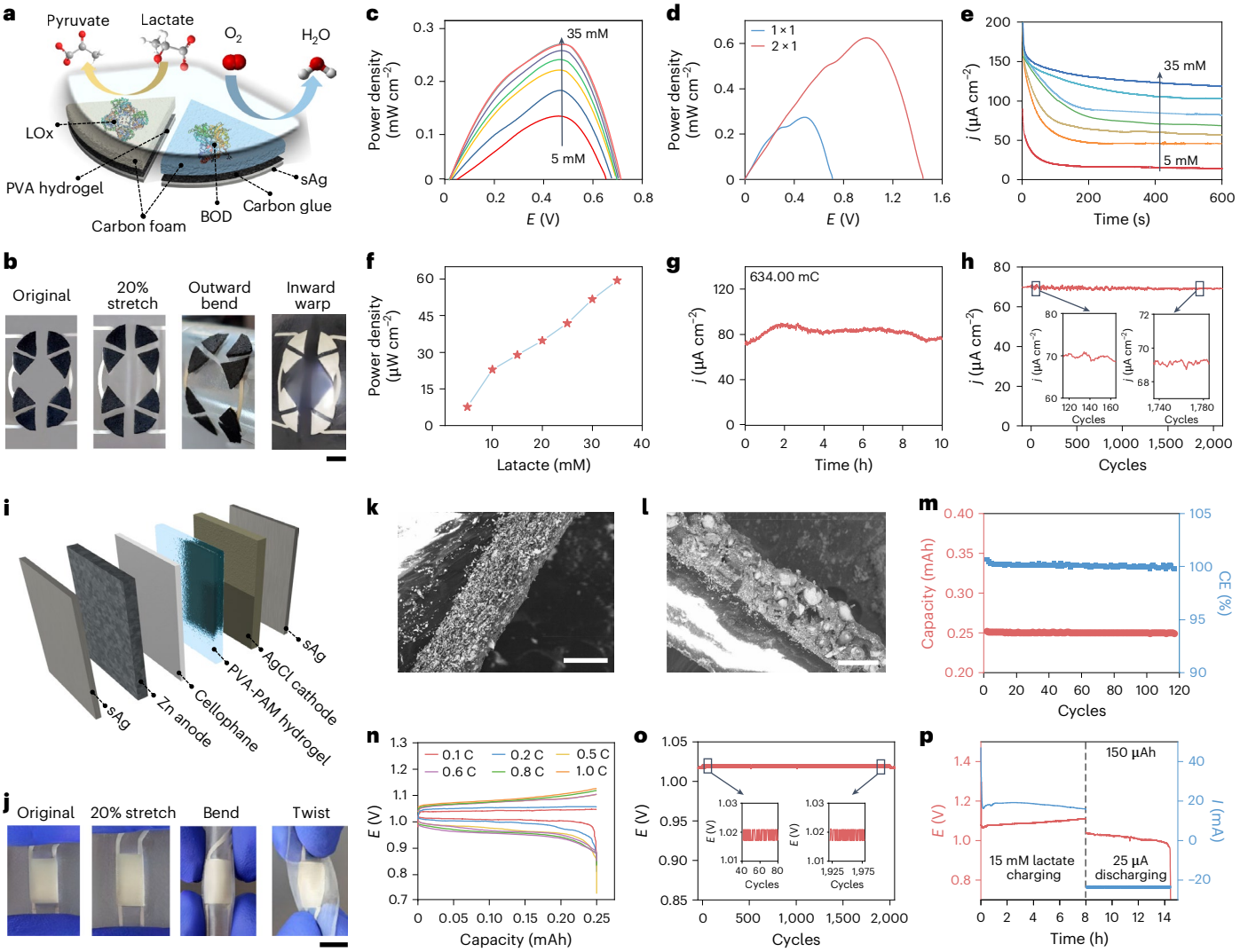

Fig. 2 | Characterization of the BFC and the flexible AgCl-Zn battery. **a**, Exploded view of the individual layers in the enzymatic BFCs. The structure of LOx and BOD is adapted from RCSB PDB number 2J6X and 2XLL. **b**, Images of the BFCs under stretching, bending and wrapping. Scale bar, 5 mm. **c**, The power density profile of a single BFC with different lactate concentrations (5 to 35 mM) after characterizing using LSV. Scan rate, 5 mV s^{-1}. **d**, The power output of a single and pair BFCs was characterized using LSV with 20 mM lactate. Scan rate, 5 mV s^{-1}. **e**,**f**, The current density of a single BFC at 0.50 V (**e**) and the power-calibration plot of the BFC with different lactate concentrations (5 to 35 mM) in 0.1 M PBS. **f**,**g**, The current density of pair BFC at 0.5 V under a 25 mM lactate concentration for 10 h. **h**, The current density of pair BFC under repeated 20% uniaxial stretching for 2,000 cycles (CA at 1 V with 25 mM lactate). **i**, Exploded view detailing the individual layers of the AgCl-Zn flexible battery. **j**, Images of the AgCl-Zn battery under 20% stretching, bending and twisting. Scale bar, 5 mm. **k**,**l**, SEM images of the AgCl cathode (scale bar, 50 μm) (**k**) and Zn anode (scale bar, 150 μm) layers (**l**). **m**, The cycling performance of the battery at charging and discharging rates of 0.4 C. **n**, The voltage–capacity plot of the AgCl-Zn flexible battery under different discharging current rates (C-rate). **o**, The battery voltage under repeated 20% uniaxial stretching for 2,000 cycles. **p**, Charging of the AgCl-Zn battery by the BFC in the presence of 15 mM lactate fuel for 8 h, followed by 25 μA current discharging. *E*, voltage; *I*, current; *j*, current density; CE, coulombic efficiency.

The capability of the BFC to withstand repeated stretching, bending and wrapping deformations was also evaluated. The current intensity underwent a minimal decay of 2.5% (of initial current) after 2,000 cycles of 20% axial stretching (Fig. 2h). Negligible changes in the BFC current density were observed even after 2,000 cycles of inward bending and wrapping (Supplementary Fig. 12), indicating that the performance of the BFCs remains largely unaffected by repeated deformations.

The AgCl-Zn battery was selected for the fingertip microgrid system owing to its matchable potential, safe pH-neutral aqueous electrolyte medium, electrochemical stability and chemical resiliency[45] .We adjusted the ink formulations and made the electrode materials compatible with the substrate, ensuring mechanical stretchability, lightweight design and user comfort. As depicted in Fig. 2i, the flexible AgCl-Zn battery relies on the following two half-cell reactions: (1) $Zn \leftrightarrow Zn^{+2} + 2e^-$, E = −0.76 V versus SHE; (2) $AgCl + e^- \leftrightarrow Ag + Cl^-$, E = +0.22 V versus SHE (SHE, standard hydrogen electrode), leading to a full cell potential of around 1 V (ref. 46). Paired batteries connected in series can support a potential of 2 V to support the electronics (Supplementary Video 1). The AgCl-Zn battery exhibits flexibility and durability when subjected to repeated mechanical deformations (Fig. 2j). The Zn anode and AgCl cathode were manufactured by a screen-printing technique, and their morphology was characterized using SEM (Fig. 2k,l and Supplementary Fig. 13). A cellophane-based film was used as a separator to help block the silver migration[47]. A polyvinyl alcohol–polyacrylamide (PVA-PAM) hydrogel, immersed with zinc sulfate ($ZnSO_4$) and potassium chloride (KCl), served as the solid electrolyte. The thermoelastomeric SEBS substrate exhibits compatibility with heat and vacuum sealing methods, enabling

reliable packaging of the battery components that effectively safeguards the electrolytes and provides the necessary protection to the system. The number of cathode layers was investigated to optimize the capacity and stability (Supplementary Fig. 14). The battery, fabricated by two printed AgCl layers was selected for the microgrid system, due to its enduring cycling performance (117 cycles) at a rate of 0.4 C (charging and discharging) without substantial capacity degradation (Fig. 2m and Supplementary Fig. 15a). It also exhibited better capacity and long life compared to the three-layer design (Supplementary Fig. 14c). The flexible battery can withstand various charging and discharging rates (ranging from 0.1 to 1 C) without compromising its overall capacity (Fig. 2n and Supplementary Fig. 15b). It also exhibited a Coulombic efficiency (CE) of ~100%, indicating efficient charge and discharge processes throughout different cycling periods (Supplementary Fig. 15a). Additionally, the battery exhibited extended capacity retention under lower depths of discharge (Supplementary Fig. 15c). The mechanical stability of the battery was evaluated under repeated 2,000 cycles of 20% uniaxial stretching, bending and twisting (Fig. 2o and Supplementary Fig. 16). The battery displayed a negligible voltage change with no capacity loss (Supplementary Fig. 17) or structural change (Supplementary Fig. 18) in both anode and cathode. Also, the 2 V in-series battery system could continuously supply power under various bending and stretching situations (Supplementary Video 1). Following the separate performance characterization of the BFC and the AgCl-Zn battery, the synergistic capabilities of these two components for extended energy harvesting and storage were examined. The performance of both the BFC and AgCl-Zn battery remained largely consistent under typical daily ambient temperatures, demonstrating the overall stability of the energy power module (Supplementary Fig. 19). Based on the designed self-regulated principle, BFCs connected in series charged the AgCl-Zn battery using a typical sweat lactate concentration of 15 mM (simulated sweat lactate concentration under active perspiration ranging from 2 to 30 mM)[48]. On connecting the fully discharged AgCl-Zn battery to the BFCs, a continuous supply of 16–19 μA current was sustained. The battery voltage consistently exceeded 1 V, undergoing continuous increase without reaching a complete charge state after 8 h. The collected energy can support a 25 μA discharge for more than 6 h, accumulating an energy capacity surpassing 150 μAh and reaching 60% of the battery's capacity (Fig. 2p).

On-finger bioenergy harvesting and battery charging

The bioenergy harvesting ability of the BFCs was thoroughly evaluated through on-finger touch measurements. Porous PVA hydrogels, tailored to match the BFC's size using a three-dimensionally printed fan-shaped hydrogel cutter (Supplementary Fig. 20a,c), were attached on top of the BFC electrodes as the sweat collection and biomarker transfer media. The hydrogel facilitates the continuous flow of natural perspiration from the skin, providing lactate to fuel the BFCs. A mode-method fabricated SEBS-based cover was designed to hold the hydrogels (Supplementary Fig. 20b,c). A rapid increase in power is observed on intermittently touching the BFC, which illustrates that BFC can be refuelled on retouching the porous PVA hydrogels (Supplementary Fig. 21a). Moreover, negligible power is generated using a plastic-covered (control) finger (Supplementary Fig. 21b), confirming the BFC energy output to be coming from only sweat lactate and not from the mechanical press or fraction. After removing the finger, the accumulated sweat within the hydrogels sustains the BFC operation, enabling continuous generation of high-density energy for at least 15 min (Fig. 3a). The harvested bioenergy by BFC also depends on the sweat accumulation time. As shown in Fig. 3b and Supplementary Fig. 22, the harvested bioenergy increases on extending the BFC touching time. This was proved by touching the PVA gel for 1 to 5 min, with a total energy generation period of 15 min. The harvesting behaviour during continuous touch was further analysed over 1 h using four different participants under desk work or at rest (Fig. 3c and Supplementary Fig. 23). The harvested power depends on the sweat lactate concentration, which can vary with individuals and the activity type (Fig. 3d). Also, the passive sweat based harvested energy was seldom affected by routine bench work. A single BFC can harvest a maximum 99.7 mC of charge and an average 72.5 mC of charge, which corresponds to an energy magnitude of 72.5 mJ. However, we found that intensive exercise tends to lower the power generation. This can be attributed to lactate dilution from excessive sweat release (Supplementary Fig. 21c) due to either increased reabsorption of lactate or decreased reabsorption of water at the sweat glands[42,49]. The long-term continuous energy harvesting ability of the BFC was further investigated under normal daytime desk work and during nighttime sleeping. The BFCs were worn on the finger and continuously measured for 4 and 8 h (Fig. 3e) during daytime and sleep, respectively (Fig. 3f). The power peaked at 20–30 min from the initial sweat with high lactate, followed by a decrease in intensity due to dilution from more sweat release. Results show that over 500 mC of charge was collected during 8 h of desk work and almost 300 mJ of energy during 8 h of sleep without exercise. It should be noted that the bioenergy levels are higher in the daytime compared to nighttime over the same testing period, which reflects that daytime finger activities enhanced fuel and oxygen diffusion rates to the BFC electrodes. These data further demonstrate the ability of BFCs to harvest energy consistently throughout various daytime activities.

After evaluating the BFC and battery performance separately, their combined performances were characterized for extended energy harvesting and storage. The BFCs were connected to the battery to evaluate their charging capability on the fingertip with different participants and scenarios. As shown in Fig. 3g, the participants wore the bioenergy module (AgCl-Zn connected with paired BFCs in series) on the fingertip for different time periods. The BFCs were able to provide stable potential throughout the testing period, but the current intensity started decaying within half an hour during the ongoing consumption of lactate. The batteries were charged by the BFCs, then disconnected and discharged. The stored energy ranged from 90 to 140 μAh (charged for 4 and 8 h, respectively), and could run ~2 and 5 h, respectively. In a different trial, the participant also wore the bioenergy module while sleeping, collecting 98 μAh of capacity overnight (Fig. 3h). Overall, on the basis of the data from three different participants, we noticed a cumulative collection of ~125 and 90 μAh charge during 8 h of day- and nighttime operation (Fig. 3i and Supplementary Fig. 24), respectively. Therefore, the bioenergy module can continuously harvest and store energy in the battery over extended periods. The bioenergy module can also simultaneously harvest energy from different fingers through rational design adjustments of the BFC and/or battery numbers and circuitry. As shown in Fig. 3j, we designed three BFC pairs in series to collect energy from three different fingers, thereby charging three AgCl-Zn batteries in series. The collected charge (125 μAh) ranged similar as the single-finger energy module (Fig. 3k). With three times enhanced voltage (~3.2 V), the collected energy is proportionally tripled. This strategy enables the on-finger energy system to support various applications with different operational voltage requirements.

Osmotic sweat enabled biochemical sensor operation

The osmotic microfluidic biochemical sensing platform comprises three major components: hydrogel, electrochemical sensor array and a paper microfluidic channel (Fig. 4a(i)). The paper channel stays sandwiched in between the hydrogel and fingertip, while the sensor array interfaces the thin rectangular section of the channel near inlet. The hydrogel is initially equilibrated with pure ethylene glycol to minimize its water content and eventually raise its osmotic strength relative to sweat[38]. Hence, on contact with the fingertip, the hydrogel withdraws sweat directly (in addition to natural perspiration) from the skin surface via osmosis in a non-invasive and exertion-free manner

https://doi.org/10.1038/s41928-024-01236-7

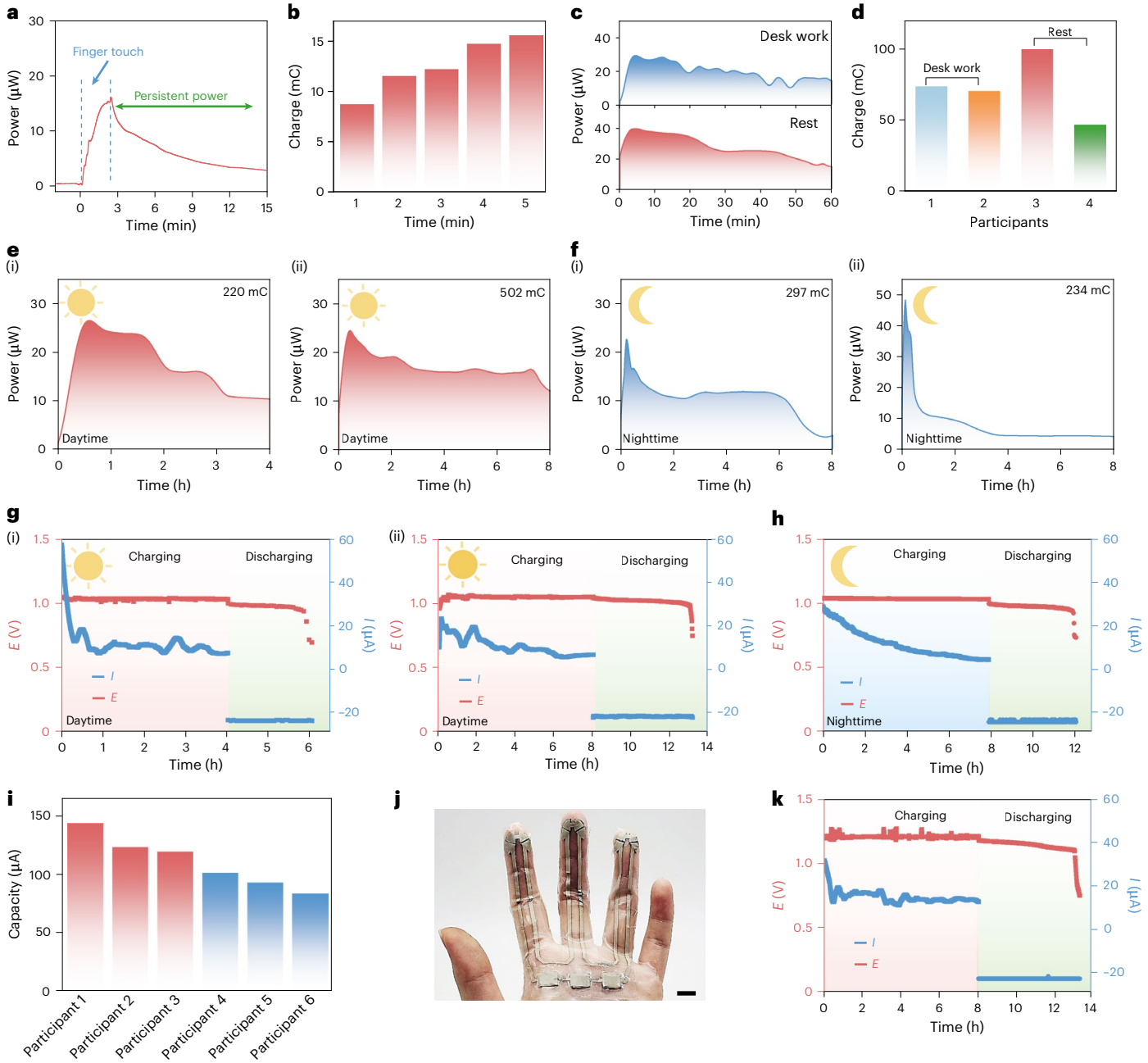

Fig. 3 | In vivo energy harvesting and charging battery. a, The acquired power trend from the BFC after touching with a finger for 2 min. **b**, Comparison of the charge collected from a single BFC with different touching times. **c**,**d**, Power profile (**c**) and charge plot (**d**) during a 1 h daytime session from different participants and scenarios. **e**, BFC passively harvested bioenergy from the fingertip during (i) 4 h and (ii) 8 h from two different participants during the daytime. **f**, BFC passively harvested bioenergy on the fingertip during nighttime (8 h of sleep) from two participants. **g**, BFC passively harvested bioenergy for (i) 4 h and (ii) 8 h from two different participants during daytime, followed by 25 μA discharging the battery. **h**, BFC passively harvested bioenergy over 8 h during nighttime, followed by 25 μA discharging the battery. **i**, The summarized battery capacities charged by the BFC after 8 h during the daytime (red) and nighttime (blue). **j**,**k**, Photograph of six BFCs on three fingers for charging three batteries in series (scale bar, 1 cm) (**j**) and passively harvesting bioenergy for 8 h, followed by 25 μA discharging of the battery (**k**). Red, blue and green backgrounds in **j**, **h** and **k** represent the charging period in daytime, nighttime and following battery discharging, respectively.

(Fig. 4a(ii)), without any external power requirement (as in iontophoresis)[38,50]. Osmotic pressure is a colligative property that keeps the sweat extraction process dependent only on the chemical potential difference between the gel and sweat. The extracted sweat flows onto the paper channel, which has a rectangular section to accommodate the sensor array, followed by a serpentine structure with a high surface area to support extended sweat collection (Fig. 4b and Supplementary Fig. 25). The hydrophilic nature of the paper allows rapid sweat transport via capillary wicking. The sensors exhibit commendable mechanical stability (negligible structural change on bending, twisting and stretching) and high sensing stability (negligible drift after 2,000 cycles of 20% stretching), making them ideal for wearable applications on the finger (Supplementary Figs. 26 and 27). In vitro testing on the fingertip showed that a hydrogel comprising a copolymer of polyvinyl alcohol and polyacrylamide functioned the best in sampling the highest amount of sweat per unit time (Fig. 4c). Hence, this hydrogel variant was used for all our on-body tests. We tested the platform for continuously monitoring four biomarkers relevant to daily life

https://doi.org/10.1038/s41928-024-01236-7

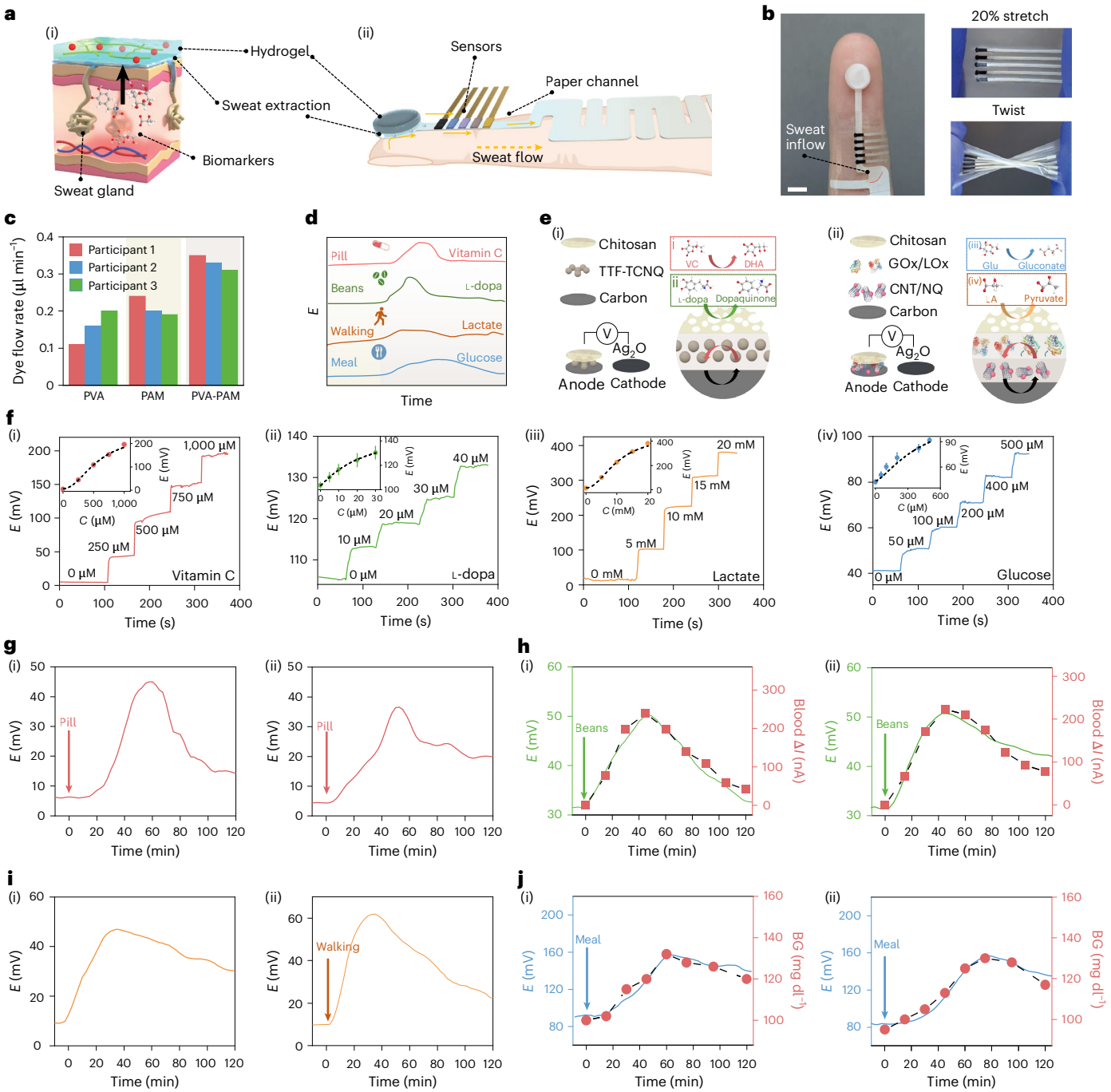

Fig. 4 | Sensor operation with osmotically withdrawn sweat. a, (i) Schematic highlighting the hydrogel interfacing the skin to facilitate sweat withdrawal with biomarkers, (ii) and the orientation of the osmotic platform with multiple sensor arrays on the fingertip. **b**, Optical image of sweat flow in the paper channel with the interfaced enzymatic sensors, and mechanical properties of sensors under stretching and twisting. Scale bar, 5 mm. **c**, Dye flow rate on the finger using different hydrogel variants. **d**, Schematic illustration of biomarker sensing with related daily activity. **e**, Schematic of potentiometric sensors of vitamin C and L-dopa (i) and enzymic sensors of glucose and lactate (ii). The structures of LOx and GOx are adapted from RCSB PDB number 2J6X and 1GAL. **f**, Plots showing in vitro sensor performance with an inset of the calibration curve for (i) vitamin C, (ii) L-dopa, (iii) lactate and (iv) glucose detection in sweat. **g**, On-finger response of the vitamin C sensor after pill intake at $t = 0$ min from two participants. **h**, On-finger response of the L-dopa sensor and blood L-dopa chronoamperometry signal from two participants after fava beans consumption. **i**, On-finger response of the lactate sensor measurements at rest using (i) a completely sedentary participant and (ii) on the same participant after 30 min of outdoor walking. **j**, On-finger response of the glucose sensor and measured blood lactate concentration after a meal intake at $t = 0$ min from two participants. BG, blood glucose concentration.

activities: vitamin C, Glu, lactate and L-dopa (Fig. 4d). The sensor comprised a two-electrode system: the anode (working electrode) was developed using carbon with oxidation supporting mediator, and the cathode (counter electrode) was made of silver oxide (Ag_2O) (Fig. 4e). The vitamin C and L-dopa sensors relied on the tetrathiafulvalene 7,7,8,8-tetracyanoquinodimethane salt (TTF-TCNQ) mediated oxidation (Fig. 4e(i) and Supplementary Fig. 28a). The operation of the glucose and lactate sensors relied on synergistic and specific NQ-mediated oxidation, along with glucose oxidase (GOx) and LOx enzymes, respectively (Fig. 4e(ii) and Supplementary Fig. 28b). The working electrode is

coupled with the Ag_2O counter electrode, which undergoes reduction to Ag (Supplementary Fig. 28c). The performance of the different sensors was first tested in vitro with artificial sweat (Fig. 4f). On applying an external load, current flows between the electrodes proportionally to the analyte concentration. The external loads for all sensors were finalized using LSV (Supplementary Fig. 29), while the effect of flow rate, pH, analyte interference, limit of detection values and control studies have been examined for each sensor (Supplementary Figs. 30–33). Overall, a lower analyte concentration demands a higher load for greater signal resolution. The vitamin Csensor was tested in vitro until 1,000 µM under 1 MΩ of load, and its performance on the body was evaluated via the intake of a pill supplement (Fig. 4g(i),(ii)). Both participants showed a potential change of ~35–45 mV, which peaked ~60 min after pill intake. No voltage change was observed in a controlled experiment without pill (Supplementary Fig. 34). The L-dopa sensor was tested in vitro until 30 µM under 10 MΩ of load and validated on the body through the consumption of fava beans[51]. Both participants showed a change of ~15–20 mV, which peaked around 45–60 min after beans intake (Fig. 4g(i),(ii)). Blood L-dopa levels were measured using established protocols (Supplementary Fig. 35)[36], showed a good correlation with the estimated sweat L-dopa levels. The lactate sensor was tested in vitro up 20 mM under 75 kΩ load, and its performance on-body was evaluated under rest and walking conditions (Fig. 4f(i),(ii)). As expected, sweat lactate response did not change at rest but increased (by roughly 25 mV) under walking. Blood lactate did not change under either condition, validating that lactate appears faster in sweat than in blood. The glucose sensor was tested in vitro until 500 µM with a 1 MΩ load and validated on-body through meal intake (Fig. 4e(i),(ii) and Supplementary Fig. 36). The sensor showed negligible change in its performance at different temperatures under the reported physiological sweat glucose concentrations (Supplementary Fig. 19c). Both participants showed a change of around 70–80 mV, which peaked in 60 min, after meal intake. The glucose response profiles correlated well with the temporal blood glucose concentration trends. Overall, the potential of this platform to continuously monitor multiple biomarkers from the fingertip sweat highlights its wide applicability towards non-invasive health monitoring.

Integrated fingertip-wearable microgrid system

An ultra-low-power MCU (nRF52832, 6 × 6 mm), capable of operating below 1.7 V and suitable for BLE, was selected for the wearable microgrid system. The BFC charging the AgCl-Zn batteries energy system generates a higher open-circuit voltage of 2 V, which can directly power the fPCB without needing a voltage booster. The MCU controls the four sensors for data input, storage and BLE transmission (Fig. 5a). To enable multiplexed sensing, the integrated system was interfaced to different resistors, tailored for acquiring maximum resolution for each sensor signal (such as vitamin C, Glu, LA and L-dopa). The MCU power consumption was further analysed during operation. The electronics functions with an average current consumption of 5 µA in idle mode with ADC operation every 30 s, and ~190, 325 and 200 µA during advertising mode, onset of paired and paired mode, respectively (Fig. 5b and Supplementary Fig. 37). The energy system is then discharged under a designed script that mimics the power consumption of the operational MCU. Here, a procedure set with continuous ADC consumption, and an interval of every 30 s has 6 s for BLE (2 s advertising mode, 1 s onset of paired and 3 s during paired mode) consumption (Supplementary Fig. 38). The fully charged batteries connected to BFCs with 25 mM lactate can greatly extend (by ~8.5 h) the runtime (by adding 240% extra capacity), compared to the bare battery without the BFCs (Fig. 5c). The MCU was further integrated on a custom-designed fPCB (Supplementary Fig. 39) (18 × 18 mm) with high flexibility and conformity on the finger (Supplementary Fig. 40a,b). Each MCU pin is 1 mm wide and has a 2 mm gap to allow convenient connections with the sensors and batteries. The MCU was further programmed with the measurement procedures from the input pins on the back side (Supplementary Fig. 40c), and then integrated with each battery and sensor module for on-body use. As the fingertip microgrid is designed for extended on-body operation, its cytocompatibility and biocompatibility are important. Figure 5d proves that each module of the microgrid system had little effect on the cell viability. Furthermore, the biocompatibility of the device was examined by incubating it in leukaemia monocytic cells (THP 1 cells) for 24 h. The cells retained their high viability over these extended periods, justifying the biocompatibility of the device components. Besides, no sign of side effects on the skin were observed within a few hours of wearing the microgrid. While extended exposure can lead to slight wrinkling of the skin, the skin typically returns to its normal condition within 10 min (Supplementary Fig. 41a).

The participant wore the microgrid system on the fingertip (Fig. 5e(i) and Supplementary Video 2) to track all four biomarker profiles throughout the day under routine activities such as desk work, meals, drinks, walking and sleeping, along with harvesting power simultaneously (Fig. 5e(ii)). The biomarker levels were translated in real-time and displayed on a custom-designed mobile or laptop web application (Fig. 5e(iii), Supplementary Fig. 42 and Supplementary Video 3). Both BFCs and osmotic hydrogel maintained intimate contact with the skin (Supplementary Figs. 41b,c and 43a). The approximate pressure exerted by each hydrogel corresponds to ~4.5 kPa (Supplementary Fig. 43b). The power consumption was also tracked, and a lower baseline with peaks was observed under 2 mW during operation (Fig. 5f(i)). Also, the energy system exhibits greater than 1.8 V operational voltage under idle, testing, and BLE transmission situations, which guarantees MCU operation for 16 h (Fig. 5f(ii)). For tracking daytime activities, the microgrid was worn in the morning, and lactate was initially monitored for 4 h during normal desk work (Fig. 5g). No major change was observed due to the absence of physical exertion. Next, the participant consumed lunch and glucose was monitored. The sweat glucose signal increased (~90 mV change) and started dropping down after 1 h. In late afternoon, the participant consumed ice cream and orange juice to monitor glucose and vitamin C simultaneously. Both glucose and vitamin C profiles showed an increasing trend, with glucose showing a net change of ~50 mV after 1 h, while vitamin C showed a net change of ~23 mV after 45 min. After this, the participant conducted an outdoor walk for 30 min while monitoring glucose and lactate levels. The glucose profile showed no change, but the lactate readout increased by ~20 mV in 30 min. Finally, the participant consumed dinner, which included fava beans. Both glucose and L-dopa levels were monitored for the next 4 h (including sleep), in which the glucose response increased by ~42 mV after 1 h, while the L-dopa response increased by ~30 mV after 30 min. Overall, the ability to conduct such continuous and extended simultaneous monitoring of multiple biomarkers via osmotic extraction, demonstrates the efficient functioning and practicality of the integrated microgrid system on the fingertip for daily activity tracking.

Conclusions

We have reported a wearable microgrid system for fingertips. The integrated microgrid combines AgCl-Zn batteries and enzymatic BFCs, with custom-designed fPCB and four electrochemical sensors for monitoring vital metabolic biomarkers and drugs (glucose, vitamin C, lactate, L-dopa) in sweat. The BFC and printed battery support bioenergy harvesting from sweat lactate and storage, respectively. The pair of BFCs can generate almost 500 mJ (daytime) and 300 mJ (nighttime) of energy and can charge the battery with 125 and 90 µAh of energy during 8 h of daytime activities and nighttime sleep, respectively. With this approach, users can passively harvest long-term bioenergy, store it with extended battery operations and use it to power the MCU, which can deliver electrochemical sensing of sweat biomarkers at rest for more than 16 h. The sensor data can also be directly acquired on a smartphone via wireless Bluetooth data transmission.

https://doi.org/10.1038/s41928-024-01236-7

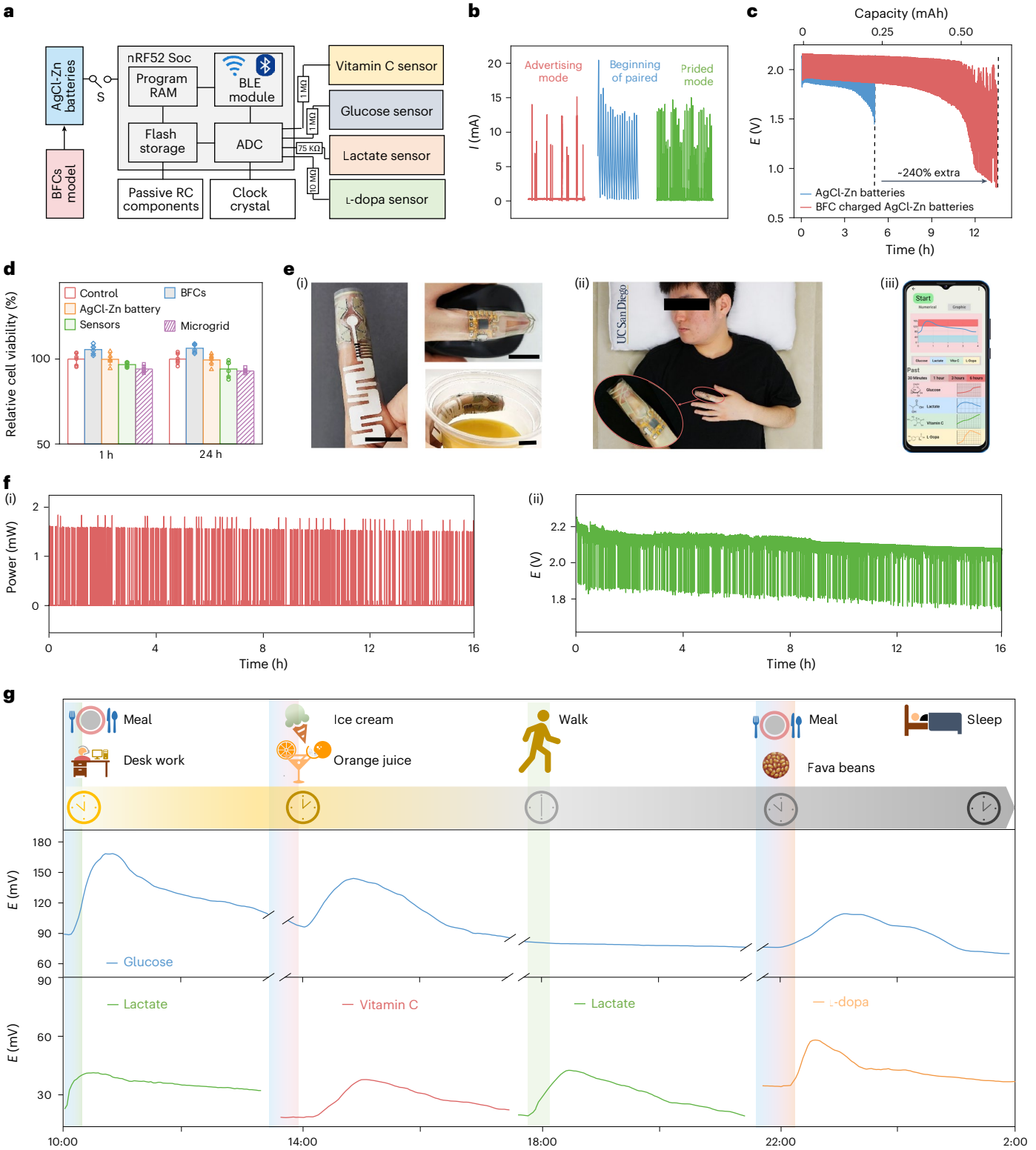

Fig. 5 | Operation of the integrated fingertip-wearable microgrid system. **a**, Block diagram of the wearable electronic system. **b**, The power consumption of MCU during BLE advertising mode, beginning of paired and paired mode. **c**, The discharge profile of two AgCl-Zn batteries connected in series implements the simulation discharge profile with and without BFCs charging. **d**, Quantitative analysis of cell viability over 1 and 24 h culture periods. Data represents mean ± s.d. ($n = 6$). **e**, Optical image of a participant wearing the fingertip microgrid during daytime activities with desk work (using the computer mouse) and drinking orange juice (i), and during nighttime sleep (ii). (iii) The collected data were wirelessly transmitted to a smartphone and displayed in the custom-designed mobile web app. Scale bar, 2 cm. **f**, Full-day cross-activity energy consumption (i) and voltage response (ii). **g**, Full-day biomarker monitoring with the wearable fingertip microgrid under varying daily activities. S, switch.

Our fingertip-wearable microgrid platform could be of use in a range of scenarios in personalized healthcare monitoring and wellness management. The performance of the on-finger microgrids could be further enhanced from common daily activities involving finger movement (such as tapping or typing) to boost the energy collection, based on additional energy harvesting techniques (such as piezoelectricity or triboelectricity). Rational design of the circuit, battery, low-power sensing modules and data transmission technologies can also collectively boost the lifespan, stability and functionality of the device, with sustained balance between the energy generation and consumption rates in the entire system.

Methods

Chemicals and reagents

Bismuth(III) oxide (Bi_2O_3), PVA (molecular weight ~30,000), SEBS, NQ, chitosan, ABTS, Ag flake, Ag_2O, glutaraldehyde, acetic acid, lactic acid, phosphate buffered saline (PBS), 2-hydroxy-4′-(2-hydroxyethoxy)-2-methylpropiophenone, poly(ethylene glycol) diglycidyl ether (PEGDE), hemin, potassium hydroxide (pellets) (KOH), sucrose, GOx, BOD, potassium peroxodisulfate ($K_2S_2O_8$), acrylamide, *N*,*N*′-methylenebisacrylamide, sodium chloride (NaCl), acetone (Ace), ethanol (EtOH), toluene, xylene, ethylene glycol, $ZnSO_4$ monohydrate, zinc oxide (ZnO), TTF-TCNQ and cellophane (gel drying frames) were all purchased from Sigma-Aldrich. Poly(vinylfluoride-co-2,3,3,3-tetrafluoropropylene) binder (GBR 6005) was acquired from Daikin US Corporation. KCl (P217-500) was obtained from Fisher Scientific. LOx was purchased from Toyobo Co., Ltd. The Zn powder was purchased from Grillo-Werke. Graphite powder was purchased from Acros Organics. Multiwall carbon nanotube (MWCNT) (90% purity) and carboxyl-functionalized one (MWCNT-COOH) were purchased from Cheap Tubes and Nanocyl, respectively. Ag/AgCl ink was acquired from Ercon Inc. Super P conductive carbon black was ordered from MTI Corp. Other two SEBS binders (G1645 and MD1648) were supported by Kraton. Polyethylene terephthalate sheeting was purchased from Polymer Innovations, Inc.

Fabrication of the stretchable circuit system

The sAg served as the circuit connection linking to different components of the fingertip microgrid. The circuit and current collector design were designed using AutoCAD 2023 (Autodesk) and transformed into a custom stencil by Metal Etch Service. The formulation of the silver ink involved blending 4 g of Ag flakes, 2 g of SEBS resin (G1645, 1:2.17 wt% dissolved in toluene) and 1 g of toluene. This mixture was made using a planetary mixer (FlackTek, Inc. SpeedMixer DAC 150.1 FVZ) set at 1,800 rpm for 10 min until homogeneous. Afterwards, the ink was screen-printed onto the doctor blade-made SEBS substrate, prepared by dissolving MD1648 in toluene (40 wt%). A NaCl:lactate (2:1, molar ratio) treatment step was performed on the printed sAg circuit, which was adapted from a previous study[37]. The prepared solution was sprayed onto the printed sAg circuit and subsequently dried in an oven at 80 °C for 5 min, repeated three times and then washed with deionized water.

Fabrication of the BFCls

Porous flexible carbon foam was fabricated at first (synthesis detail in Supplementary Information), then cut into eight 0.213 cm^2 fan-shaped sectors and affixed onto the silver current collectors using carbon glue. Here, carbon glue was made by mixing Super P conductive carbon black, graphite, SEBS binder (2 g of Sigma SEBS in 0.87 g of toluene) in a 0.5/3/4.2 weight ratio. The ABTS and CNT mixture was prepared by mixing 25 ml of 20 mM ABTS in deionized water with 60 mg of MWCNT-COOH and boiled at 140 °C overnight, then filtered and washed with deionized water, as well as dried at 120 °C for 1 h. Subsequently, each of the cathodes (0.213 cm^2) were drop casted with 50 µl of ABTS/CNT dispersion (2 mg ml^{-1} in EtOH/Ace (1:4, v/v) solution), 15 µl of hemin (40 mM in 1 wt% of GBR 6005-Ace solution), 15 µl of BOD (20 mg ml^{-1} in 0.1 M PBS) and 5 µl of 1% PEGDE (1 wt% in deionized water). The NQ/CNT mixture was prepared by dispersing 100 mM of NQ with 2 mg of MWCNT-COOH in 1 ml of EtOH/Ace (1:4, v/v) solution. Next, each of the anodes were drop casted with 50 µl of NQ/CNT dispersion, 115 µl of LOx (20 mg ml^{-1} in 0.1 M PBS), 5 µl of 1% glutaraldehyde (1 wt% in deionized water) and 5 µl of 1% chitosan (0.1 g in acetic acid (0.1895 ml) and deionized water (10 ml) solution. Each new layer was drop casted subsequently once the previous layer had dried entirely. The resulting BFCs were then stored in the refrigerator for later usage.

Fabrication of the stretchable AgCl-Zn battery

The formulations of the battery inks and electrolytes were derived and adjusted on the basis of previous research and established studies[17]. Each battery had dimensions of 1 × 0.7 cm, resulting in a surface area of 0.7 cm^2. The Zn anode ink was prepared by thoroughly grinding Zn powder, ZnO and Bi_2O_3 in a 10/0.5/0.5 weight ratio ensuing by mixing in a 4/1 weight ratio with the GBR binder (26.67 wt% of GBR 6005 in Ace), and then undergoing a strong mixing step in a planetary mixer at 1,800 rpm for 5 min until homogeneous. Similarly, cathode ink was prepared by combining Ag/AgCl ink with GBR binder in a 2/1 weight ratio and mixing at 2,250 rpm for 5 min until the desired consistency was obtained. Both inks were screen-printed onto the sAg current collectors prepared on the SEBS substrate. The 1.5 M $ZnSO_4$ and 0.5 M KCl solution-soaked PAM-PVA gel (synthesis detail in Supplementary Information) was used as the solid electrolyte. The stretchable battery was then assembled with the following configuration in a stacked manner: SEBS, Zn anode, cellophane, PAM-PVA gel, AgCl cathode and then SEBS.

Fabrication of the sensors

All sensors were composed of a two-electrode system, which was composed of four anodes and one shared cathode. Initially, five sAg current collectors were screen-printed on the SEBS substrate. The anode (4 × 1 mm) was prepared using carbon ink based on our previous study[52] and was screen-printed on the four ends of a current collector. The cathode (4 × 1 mm) was prepared on the first end of the collectors by screen-printing a subsequent layer of Ag_2O ink over the carbon ink. Each layer after printing was cured at 80 °C for 15 min. The carbon ink formulation consisted of Super P carbon black, graphite, SEBS G1645 (dissolved at 40 wt% in toluene), and toluene, combined in a weight ratio of 6.0/1.0/8.4/2.1. The Ag_2O ink was formulated by combining Ag_2O, Super P carbon black and GBR binder (dissolved at 21 wt% in acetone) in a weight ratio of 1.900/0.100/3.166. All the inks were blended at 2,500 rpm for 10 min via a planetary mixer, ensuring a homogeneous consistency. The junction between the current collector and the printed electrodes was insulated before usage.

The glucose sensor was prepared by drop casting sequentially 5, 5, 1 and 1 µl of NQ solution (0.2 M) (solvent composed of 2 mg ml^{-1} MWCNT-CCOH in 1:9 EtOH to Ace), 40 mg ml^{-1} GOx solution, 1% glutaraldehyde in deionized water and 1% chitosan in 0.1 M acetic acid on an anode electrode. An external resistor of 1 MΩ was soldered between the two electrodes as the discharge load. The lactate sensor was developed by drop casting sequentially 5, 5, 1 and 1 µl of 0.2 M NQ solution (solvent composed of 2 mg ml^{-1} MWCNT-COOH in 1:9 EtOH to Ace), 40 mg ml^{-1} LOx solution, 1% glutaraldehyde in deionized water and 1% chitosan in 0.1 M acetic acid on an anode electrode. An external resistor of 75 kΩ was soldered between the two electrodes as the discharge load. For the vitamin C and L-dopa sensors, both were prepared by drop casting sequentially 5 and 1 µl of TTF-TCNQ in a 1:9 EtOH:Ace mixture and 1% chitosan in 0.1 M acetic acid on anode electrodes, respectively. The external discharge load used with vitamin C and L-dopa sensor were 1 and 10 MΩ, respectively. All external loads were finalized through LSV of the full cell at a scan rate of 1 mV s^{-1}. The intakes of different analytes in the body were conducted once all four sensors had reached a stable discharge potential.

Electrical circuit design description

The circuit comprised the MCU (nRF52832-QFAA-R, Nordic Semiconductor) and its passive support components. The circuit used a 2.4 GHz Bluetooth chip antenna (2450AT18A100E, Johanson Technology) to provide wireless capabilities in a very small form-factor. The PCB was made of a flexible substrate to better conform to the hand, and had electro-deposited copper and ENIG coating for corrosion resistance. The PCB was designed in KiCad and was manufactured and assembled by JLCPCB. The PCB design is shown in Supplementary Fig. 40. The MCU has a built-in ADC and reads data from the four unique sensors, logs them and sends those logs to a local smartphone via Bluetooth.

Assembly of fingertip microgrid system

The length of the interconnected circuits between each of the modules was custom-designed on the basis of the dimensions of the user's finger, allowing the final assembled wearable microgrid to be comfortably worn on the finger and be tightly attached to a fingertip. The printed circuit was connected to the fPCB through a 'solvent-welding' strategy from previous studies[53]. In particular, 5 and 2 µl droplets of toluene and EtOH (4:6, v/v) were used to soften the interconnecting sAg traces. Then, the fPCB was placed for sensors and batteries connection footprints, respectively. The connection points were pressed for 15 min to allow the solvent evaporation and facilitate the solid connected sAg ink with metal footprints (Supplementary Fig. 6).

The BFCs module combined four cut PVA hydrogels and a designed fingertip microgrid SEBS cover (design and fabrication details in the Supplementary Information). The biosensor module combined four major components: fingertip microgrid SEBS cover, osmotic hydrogel, electrochemical biosensors and a paper microfluidic channel (Whatman grade no. 1) (Fig. 4a(ii)). The serpentine design of the paper channel was cut out using a CO_2 laser cutter, such that its circular inlet stayed sandwiched between the hydrogel and skin, while the sensors were adhered to the thin rectangular section of the paper channel. The withdrawn sweat by the hydrogel initially travelled through the rectangular section of the paper channel, interacted with the interfaced sensors and then travelled across to the extended section of the channel.

On-body bioenergy collection and sweat sensing

All on-body trials were conducted on the basis of an approved Institutional Review Board protocol (no. 130003, UCSD). For bioenergy harvesting-storage experiments, the BFCs or BFC-battery assembly was attached to the fingertip, and data were collected with an Autolab potentiostat (PGSTAT128N). The stored bioenergy was discharged with 25 µA of discharging current. For biosensing experiments, the fingertip area was initially cleaned using alcohol wipes and deionized water before placing the wearable sensor patch. After placing the patch, it took about 15–30 min for the sweat to reach the sensor (reflecting the varying sweat rates in different individuals). The lactate and vitamin C sensors reached a stable discharge potential within 10 min, while it took around 45–60 min for the glucose and L-dopa sensors to reach their stable discharge potential. Overall, the biomarker sensing was possible after ~60 min after interfacing the osmotic hydrogel to the skin. Glucose was spiked with meal consumption and blood glucose was measured every 15 min through fingerpick testing. Lactate was spiked with an outdoor walk. Vitamin C was spiked with a pill (2,000 mg) and a commercial orange juice (containing 540 mg of vitamin C). L-dopa was spiked by consuming ~100 g of fava beans. For wearable microgrid testing, data were sampled by the fPCB and transmitted to a laptop or smartphone wirelessly via Bluetooth at a sampling interval of 30 s and a transmit interval of 5 min.

Reporting summary

Further information on research design is available in the Nature Portfolio Reporting Summary linked to this article.

Data availability

The data that support the findings of this study are available from the corresponding author upon request.

Code availability

The code for programming the MCU is available from the corresponding author upon request.

References

1. Bariya, M., Nyein, H. Y. Y. & Javey, A. Wearable sweat sensors. *Nat. Electron.* **1**, 160–171 (2018).
2. Someya, T. & Amagai, M. Toward a new generation of smart skins. *Nat. Biotechnol.* **37**, 382–388 (2019).
3. Wang, W. et al. Neuromorphic sensorimotor loop embodied by monolithically integrated, low-voltage, soft e-skin. *Science* **380**, 735–742 (2023).
4. Chen, C., Ding, S. & Wang, J. Digital health for aging populations. *Nat. Med.* **29**, 1623–1630 (2023).
5. Kim, J., Campbell, A. S., de Ávila, B. E.-F. & Wang, J. Wearable biosensors for healthcare monitoring. *Nat. Biotechnol.* **37**, 389–406 (2019).
6. Gao, W. et al. Fully integrated wearable sensor arrays for multiplexed in situ perspiration analysis. *Nature* **529**, 509–514 (2016).
7. Hu, H. et al. A wearable cardiac ultrasound imager. *Nature* **613**, 667–675 (2023).
8. Kim, J. et al. Battery-free, stretchable optoelectronic systems for wireless optical characterization of the skin. *Sci. Adv.* **2**, e1600418 (2016).
9. Jiang, Y. et al. Wireless, closed-loop, smart bandage with integrated sensors and stimulators for advanced wound care and accelerated healing. *Nat. Biotechnol.* **41**, 652–662 (2023).
10. Shirzaei Sani, E. et al. A stretchable wireless wearable bioelectronic system for multiplexed monitoring and combination treatment of infected chronic wounds. *Sci. Adv.* **9**, eadf7388 (2023).
11. Nair, V. et al. Miniature battery-free bioelectronics. *Science* **382**, eabn4732 (2023).
12. Larcher, D. & Tarascon, J. M. Towards greener and more sustainable batteries for electrical energy storage. *Nat. Chem.* **7**, 19–29 (2015).
13. Gao, M. et al. Power generation for wearable systems. *Energy Environ. Sci.* **14**, 2114–2157 (2021).
14. Gong, S. & Cheng, W. Toward soft skin-like wearable and implantable energy devices. *Adv. Energy Mater.* **7**, 1700648 (2017).
15. Song, Y., Mukasa, D., Zhang, H. & Gao, W. Self-powered wearable biosensors. *Acc. Mater. Res.* **2**, 184–197 (2021).
16. Yin, L. et al. High performance printed AgO-Zn rechargeable battery for flexible electronics. *Joule* **5**, 228–248 (2021).
17. Yin, L. et al. Wearable E-skin microgrid with battery-based, self-regulated bioenergy module for epidermal sweat sensing. *Adv. Energy Mater.* **13**, 2203418 (2023).
18. Yin, L. et al. A self-sustainable wearable multi-modular E-textile bioenergy microgrid system. *Nat. Commun.* **12**, 1542 (2021).
19. Yu, Y. et al. Biofuel-powered soft electronic skin with multiplexed and wireless sensing for human-machine interfaces. *Sci. Robot.* **5**, eaaz7946 (2020).
20. Yin, L. et al. A passive perspiration biofuel cell: high energy return on investment. *Joule* **5**, 1888–1904 (2021).
21. Garland, N. T., Kaveti, R. & Bandodkar, A. J. Biofluid-activated biofuel cells, batteries, and supercapacitors: a comprehensive review. *Adv. Mater.* **35**, 2303197 (2023).
22. Yin, L., Kim, K. N., Trifonov, A., Podhajny, T. & Wang, J. Designing wearable microgrids: towards autonomous sustainable on-body energy management. *Energy Environ. Sci.* **15**, 82–101 (2022).

23. Bandodkar, A. J. et al. Soft, stretchable, high power density electronic skin-based biofuel cells for scavenging energy from human sweat. *Energy Environ. Sci.* **10**, 1581–1589 (2017).
24. Ates, H. C. et al. End-to-end design of wearable sensors. *Nat. Rev. Mater.* **7**, 887–907 (2022).
25. Min, J. et al. An autonomous wearable biosensor powered by a perovskite solar cell. *Nat. Electron.* **6**, 630–641 (2023).
26. Song, Y. et al. 3D-printed epifluidic electronic skin for machine learning–powered multimodal health surveillance. *Sci. Adv.* **9**, eadi6492 (2023).
27. Wang, M. et al. A wearable electrochemical biosensor for the monitoring of metabolites and nutrients. *Nat. Biomed. Eng.* **6**, 1225–1235 (2022).
28. Min, J. et al. Skin-interfaced wearable sweat sensors for precision medicine. *Chem. Rev.* **123**, 5049–5138 (2023).
29. Saha, T. et al. Wearable electrochemical glucose sensors in diabetes management: a comprehensive review. *Chem. Rev.* **123**, 7854–7889 (2023).
30. Lv, J. et al. Sweat-based wearable energy harvesting-storage hybrid textile devices. *Energy Environ. Sci.* **11**, 3431–3442 (2018).
31. Ding, S. et al. Wearable microgrids empowered by single-atom materials. *Innov. Mater.* **1**, 100023 (2023).
32. Bariya, M. et al. Glove-based sensors for multimodal monitoring of natural sweat. *Sci. Adv.* **6**, eabb8308 (2020).
33. Taylor, N. A. S. & Machado-Moreira, C. A. Regional variations in transepidermal water loss, eccrine sweat gland density, sweat secretion rates and electrolyte composition in resting and exercising humans. *Extrem. Physiol. Med.* **2**, 4 (2013).
34. Brunmair, J. et al. Finger sweat analysis enables short interval metabolic biomonitoring in humans. *Nat. Commun.* **12**, 5993 (2021).
35. Sempionatto, J. R., Moon, J.-M. & Wang, J. Touch-based fingertip blood-free reliable glucose monitoring: personalized data processing for predicting blood glucose concentrations. *ACS Sens.* **6**, 1875–1883 (2021).
36. Moon, J.-M. et al. Non-invasive sweat-based tracking of L-dopa pharmacokinetic profiles following an oral tablet administration. *Angew. Chem. Int. Ed.* **60**, 19074–19078 (2021).
37. Lv, J. et al. Printable elastomeric electrodes with sweat-enhanced conductivity for wearables. *Sci. Adv.* **7**, eabg8433 (2021).
38. Saha, T. et al. Wireless wearable electrochemical sensing platform with zero-power osmotic sweat extraction for continuous lactate monitoring. *ACS Sens.* **7**, 2037–2048 (2022).
39. Milton, R. D., Giroud, F., Thumser, A. E., Minteer, S. D. & Slade, R. C. T. Bilirubin oxidase bioelectrocatalytic cathodes: the impact of hydrogen peroxide. *Chem. Commun.* **50**, 94–96 (2014).
40. Chen, X. et al. Stretchable and flexible buckypaper-based lactate biofuel cell for wearable electronics. *Adv. Funct. Mater.* **29**, 1905785 (2019).
41. Wang, C. et al. Monitoring of the central blood pressure waveform via a conformal ultrasonic device. *Nat. Biomed. Eng.* **2**, 687–695 (2018).
42. Derbyshire, P. J. et al. Lactate in human sweat: a critical review of research to the present day. *J. Physiol. Sci.* **62**, 429–440 (2012).
43. ÅStrand, I. Lactate content in sweat. *Acta Physiol. Scand.* **58**, 359–367 (1963).
44. Buono, M. J., Lee, N. V. L. & Miller, P. W. The relationship between exercise intensity and the sweat lactate excretion rate. *J. Physiol. Sci.* **60**, 103–107 (2010).
45. Liang, G. et al. Commencing mild Ag–Zn batteries with long-term stability and ultra-flat voltage platform. *Energy Storage Mater.* **25**, 86–92 (2020).
46. Bratsch, S. G. Standard electrode potentials and temperature coefficients in water at 298.15 K. *J. Phys. Chem. Ref. Data* **18**, 1–21 (1989).
47. Scharf, J. et al. Investigating degradation modes in Zn-AgO aqueous batteries with in situ X-ray micro computed tomography. *Adv. Energy Mater.* **11**, 2101327 (2021).
48. Van Hoovels, K. et al. Can wearable sweat lactate sensors contribute to sports physiology? *ACS Sens.* **6**, 3496–3508 (2021).
49. Jia, W. et al. Epidermal biofuel cells: energy harvesting from human perspiration. *Angew. Chem. Int. Ed.* **52**, 7233 (2013).
50. Saha, T., Fang, J., Mukherjee, S., Dickey, M. D. & Velev, O. D. Wearable osmotic-capillary patch for prolonged sweat harvesting and sensing. *ACS Appl. Mater. Inter.* **13**, 8071–8081 (2021).
51. Nyein, H. Y. Y. et al. A wearable patch for continuous analysis of thermoregulatory sweat at rest. *Nat. Commun.* **12**, 1823 (2021).
52. Yin, L. et al. A stretchable epidermal sweat sensing platform with an integrated printed battery and electrochromic display. *Nat. Electron.* **5**, 694–705 (2022).
53. Sempionatto, J. R. et al. An epidermal patch for the simultaneous monitoring of haemodynamic and metabolic biomarkers. *Nat. Biomed. Eng.* **5**, 737–748 (2021).

Acknowledgements

This work was supported by the UCSD Center for Wearable Sensors and Samsung. We thank the Kraton Corporation for providing all the SEBS samples.

Author contributions

J.W., S.D., T.S. and L.Y. conceived the idea and designed the experiments. S.D. and T.S. conducted the experiments. J.W. supervised the work. S.D., T.S., L.Y., R.L., M.I.K., A.-Y.C., H.L., J.Z., C.C., Z.L., C.Z., S.E., S.T., O.D., X.C., M.L., S.S.S., J.-M.M., C.M. and P.N. performed the experiments. H.Z. and Y.L. contributed to the signal processing and app development. A.S.N. designed and programmed the electronics. Y.P., K.M., S.X. and J.W. provided suggestions for the experiment designs. S.D., T.S., L.Y. and J.W. wrote the paper with the assistance of the other coauthors.

Competing interests

The authors declare no competing interests.

Additional information

Supplementary information The online version contains supplementary material available at https://doi.org/10.1038/s41928-024-01236-7.

Correspondence and requests for materials should be addressed to Joseph Wang.

Peer review information *Nature Electronics* thanks Haibo Huang, Liping Xie and Hao Sun for their contribution to the peer review of this work.

nature portfolio

Corresponding author(s): Joseph Wang

Last updated by author(s): Jul 6, 2024

Reporting Summary

Nature Portfolio wishes to improve the reproducibility of the work that we publish. This form provides structure for consistency and transparency in reporting. For further information on Nature Portfolio policies, see our Editorial Policies and the Editorial Policy Checklist.

Statistics

For all statistical analyses, confirm that the following items are present in the figure legend, table legend, main text, or Methods section.

n/a	Confirmed
☐	☒ The exact sample size (*n*) for each experimental group/condition, given as a discrete number and unit of measurement
☐	☒ A statement on whether measurements were taken from distinct samples or whether the same sample was measured repeatedly
☒	☐ The statistical test(s) used AND whether they are one- or two-sided *Only common tests should be described solely by name; describe more complex techniques in the Methods section.*
☒	☐ A description of all covariates tested
☒	☐ A description of any assumptions or corrections, such as tests of normality and adjustment for multiple comparisons
☐	☒ A full description of the statistical parameters including central tendency (e.g. means) or other basic estimates (e.g. regression coefficient) AND variation (e.g. standard deviation) or associated estimates of uncertainty (e.g. confidence intervals)
☒	☐ For null hypothesis testing, the test statistic (e.g. *F*, *t*, *r*) with confidence intervals, effect sizes, degrees of freedom and *P* value noted *Give P values as exact values whenever suitable.*
☒	☐ For Bayesian analysis, information on the choice of priors and Markov chain Monte Carlo settings
☒	☐ For hierarchical and complex designs, identification of the appropriate level for tests and full reporting of outcomes
☒	☐ Estimates of effect sizes (e.g. Cohen's *d*, Pearson's *r*), indicating how they were calculated

Our web collection on statistics for biologists contains articles on many of the points above.

Software and code

Policy information about availability of computer code

Data collection	Segger Embedded Studio was used to program the microcontroller. JavaScript was used to design Web App for sensor data collection. Landt Instruments Battery Test Equipment was used for battery data collection. Metrohm Autolab potentiostats/galvanostats instrument, Gamry Instrument, Palmsense Instrument were used for other biofuel cell and sensor data collection.
Data analysis	Origin 2021 was used to analyze and plot the data. JavaScript was used to analyze and plot the data for Web app.

For manuscripts utilizing custom algorithms or software that are central to the research but not yet described in published literature, software must be made available to editors and reviewers. We strongly encourage code deposition in a community repository (e.g. GitHub). See the Nature Portfolio guidelines for submitting code & software for further information.

Data

Policy information about availability of data

All manuscripts must include a data availability statement. This statement should provide the following information, where applicable:

- Accession codes, unique identifiers, or web links for publicly available datasets
- A description of any restrictions on data availability
- For clinical datasets or third party data, please ensure that the statement adheres to our policy

The data that support the plots within this paper and other findings of this study are available from the corresponding author upon request.

Research involving human participants, their data, or biological material

Policy information about studies with human participants or human data. See also policy information about sex, gender (identity/presentation), and sexual orientation and race, ethnicity and racism.

Reporting on sex and gender	The participants are 9 healthy adults including 7 males and 2 females.
Reporting on race, ethnicity, or other socially relevant groupings	5 participants are from East Asia, 4 participants are from South and Southeast Asia
Population characteristics	Healthy subjects with no mental disorder and skin allergies were recruited. Inclusion criterias were: aged 20–40 years; BMI between 18–40 kg m-2; no mental disorder.
Recruitment	Participating subjects were recruited from the UCSD campus by word of mouth. 9 healthy subjects (7 males and 2 females, age range 20–40 years) were included in this study. The participants were healthy without any anxiety nor depression issues. All subjects gave written informed consent before participation in the study. There were no self-selection biases or other biases
Ethics oversight	Institutional Review Board at the University of California San Diego (#130003)

Note that full information on the approval of the study protocol must also be provided in the manuscript.

Field-specific reporting

Please select the one below that is the best fit for your research. If you are not sure, read the appropriate sections before making your selection.

☒ Life sciences ☐ Behavioural & social sciences ☐ Ecological, evolutionary & environmental sciences

For a reference copy of the document with all sections, see nature.com/documents/nr-reporting-summary-flat.pdf

Life sciences study design

All studies must disclose on these points even when the disclosure is negative.

Sample size	For on body evaluation of the wearable microgrid, 9 healthy subjects were recruited. Sample sizes were chosen on the basis of literature standards for proof-of-concept experiments
Data exclusions	No data exclusion.
Replication	All replication attempts were successful when following the device fabrication process described in the paper.
Randomization	The device was fabricated with same process and was tested in all participants under same conditions. Randomization was therefore not relevant to the study.
Blinding	Not relevant, because a blinding process wouldn't influence the result.

Reporting for specific materials, systems and methods

We require information from authors about some types of materials, experimental systems and methods used in many studies. Here, indicate whether each material, system or method listed is relevant to your study. If you are not sure if a list item applies to your research, read the appropriate section before selecting a response.

Materials & experimental systems

n/a	Involved in the study
☒	☐ Antibodies
☐	☒ Eukaryotic cell lines
☒	☐ Palaeontology and archaeology
☒	☐ Animals and other organisms
☒	☐ Clinical data
☒	☐ Dual use research of concern
☒	☐ Plants

Methods

n/a	Involved in the study
☒	☐ ChIP-seq
☒	☐ Flow cytometry
☒	☐ MRI-based neuroimaging

Eukaryotic cell lines

Policy information about cell lines and Sex and Gender in Research

Cell line source(s)	Human macrophage-like cells (THP-1) was obtained from American Type Culture Collection (TIB-202)
Authentication	Cells were used without modification after receiving from the supplier and therefore were not authenticated.
Mycoplasma contamination	The cell line was tested monthly to be negative for mycoplasma contamination.
Commonly misidentified lines (See ICLAC register)	N/A

Plants

Seed stocks	N/A
Novel plant genotypes	N/A
Authentication	N/A